

Original Research

Estimation and Mapping of Aboveground Vegetation Water Storage in Jiuzhaigou Nature Reserve Using Sentinel Imagery

Junjie Lei^{1,2,3}, Wunian Yang^{1,3*}, Xin Yang^{1,3}

¹College of Earth Science, Chengdu University of Technology, Chengdu, 610059, China

²College of Surveying and Planning, Shangqiu Normal University, Shangqiu 476000, China

³Laboratory of Earth-Science Spatial Information Technology of Ministry of Land and Resources of P.R. China, Chengdu University of Technology, Chengdu 610059, China

Received: 4 April 2022

Accepted: 29 September 2022

Abstract

In order to scientifically evaluate water resource reserves and the regulation mechanisms of vegetation in a hydrological cycle, it is necessary to improve the inversion accuracy of aboveground vegetation water storage (AVWS). To calculate more accurate AVWS, Sentinel-1 (S1) and Sentinel-2 (S2) imagery were used to map the AVWS of the Jiuzhaigou Nature Reserve. Predictors extracted from S1 and S2 imagery were divided into three modelling groups: S1 data (S1G), S2A data (S2G) and S12G data (combining S1G and S2G). The best linear model (LM) and Random Forest (RF) regression model of AVWS were established by predictors of the three groups; finally, RF regression models based on S2G (10-fold cross-validation determination coefficients [R^2] = 0.67, relative root mean square error [rRMSE] = 13.78 %) and S12G (R^2 = 0.72, rRMSE = 11.94 %) were selected for mapping AVWS in the study area. The results show that the aboveground vegetation water storage (AVWS) of the study area could be effectively estimated and mapped based on synergistic predictors derived from S1 and S2, as well as S12G predictors (cooperating with S1G and S2G).

Keywords: hydrological function of vegetation, vegetation water content storage, Sentinel-1, Sentinel-2, random forest

Introduction

Vegetation water content (VWC) is widely regarded as an important characteristic of plant physiology [1], environmental water budget, and water stress [2]; it is also the main factor limiting plants' transpiration

[3] and carbon accumulation [4]. The VWC can buffer, distribute, and regulate precipitation and is an important link in the hydrological cycle; as such, it has become a topic of research interest [5]. Moreover, the VWC is an important environmental variables for evaporation and transpiration at the interface between the land and atmosphere [6]. Studying the VWC is of great significance for the quantitative study of the hydrological cycle and precipitation distribution, and it will promote research on various topics,

*e-mail: ywn@cdut.edu.cn

including environmental protection [7], forest fires [8], agriculture and forestry [9], and drought [10]. However, aboveground vegetation water storage (AVWS) is a better quantification of aboveground VWC. AVWS is VWC of aboveground vegetation based on the full consideration of the biomass and geometry (e.g., tree height) of the stems, branches, and foliage of vegetation.

From studies on VWC based on remote sensing, a number of methods have been developed, including: (1) spectral vegetation index methods [11], (2) radar vegetation index methods [12], (3) the PROSPECT model [13], PROSAIL (using coupled SAIL/PROSPECT-5 models) model [14], (4) Multiply leaf equivalent water thickness (LEWT) by leaf area index (LAI) to get Canopy Equivalent Water Thickness (CEWT) [15], (5) intelligent algorithms [16], and (6) the grey-level cooccurrence matrix method (GLCM) [17]. Sentinel-1 (S1) Synthetic aperture radar (SAR) and Sentinel-2 (S2) imagery have recently been used for VWC inversion [14], and a software module was designed for generating VWC maps with S2 data [18]. Microwave backscatter is sensitive to variations in VWC in vegetated areas [6], and SAR interferometric coherence can be used for indirect inversion of tree moisture in forested

areas De Zan et al. (2018); therefore, S1 data have been used for the inversion of vegetation parameters [20]. VWC with higher inversion accuracy is needed to enhance water content research. The inversion of VWC by the vegetation index method is based on the spectrum of the canopy surface layer; however, there is a saturation problem in vegetation indices composed of two characteristic bands [21]. For the water content of aboveground vegetation, we should consider the biomass and geometry (e.g., tree height) of vegetation stems, branches, and foliage. Research has shown that the inversion accuracy of plant parameters (e.g., biomass) can be improved by dividing the parameters into stem, branch, and foliage parameters, and then using their sum as the total parameters [22].

This study aimed to evaluate the ability of S1 and S2 imagery for the inversion and predictive mapping of AVWS, using the Jiuzhaigou Nature Reserve as a test area. To compare with previous VWC quantitative remote sensing studies and improve AVWS accuracy, this study divided the field-measured plot-scale AVWS into the stem, branch, and foliage water contents of trees. We modelled the relationships among the field-measured plot-scale AVWS, and SIG predictors

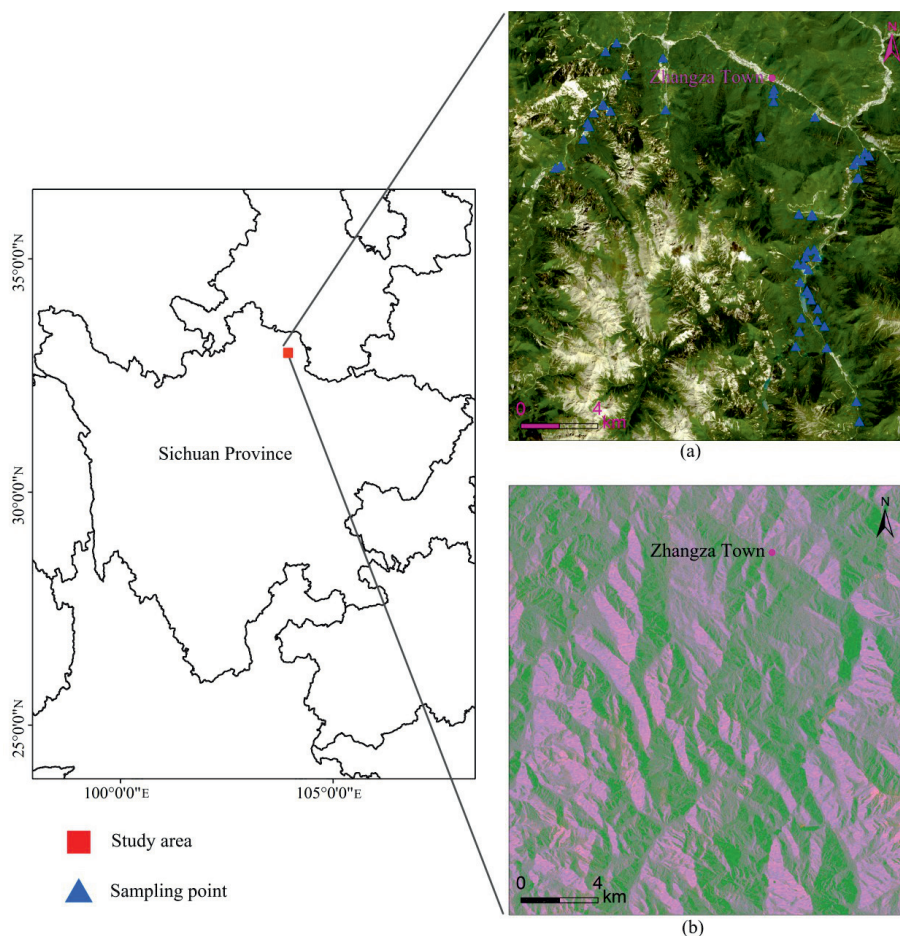


Fig. 1. Location of the study area in Jiuzhaigou County; a) S2 image acquired on 23 August 2018 in true colour composite (RGB = band4, band3, band2). b) S1 image acquired on 25 August 2018 in colour composite (RGB = VV[σ_0 , dB], VH/VV[σ_0 , dB], VH[σ_0 , dB]).

(polarisation channels [i.e., VH and VV] and their ratio [VH/VV]), and S2G predictors ([S2-derived vegetation indices, and S2-derived vegetation cover biophysical measures]), and S12G predictors. Finally, we evaluated the accuracy of the AVWS prediction model and subsequent AVWS prediction map. The novelty of this study is the use of S1 and S2 imagery in the estimation and mapping of the AVWS. This study will contribute to the development of remote sensing-based mapping technology for vegetation water content prediction.

Materials and Methods

Study Site

Jiuzhaigou is located in the transition zone between the northeast Qinghai-Tibet Plateau, Sichuan Basin, and West Sichuan Plateau (Fig. 1). The study area is located in the western Sichuan Plateau, and the terrain fluctuates significantly; higher mountains can lead to the existence of shadow and lay-over in SAR images, which results in low accuracy quantitative inversion. The region is mainly forestland and so represents an excellent case study for the AVWS of forests. Sample plots were all located in the Jiuzhaigou Nature Reserve. According to the results of field investigations by Zhang et al. (2019), the surface cover types in the study area were divided into 7 categories (Fig. 2).

All measurements (e.g., tree diameter, height) required for biomass determination were undertaken in 10 x 10 m plots. Fresh plant samples, including

branches, stems, and foliage, and shrubs and grasses, were used to measure the water content in a 1-m² quadrant. In total, 50 plots were established, of which 15 were in evergreen forest, 14 in deciduous forest, 15 in mixed forest, 4 in composite shrub grassland, and 2 in grassland. In each sample plot, hand-held GPS receivers were used to record geographic coordinates.

Methodology

Vegetation Water Content

Data on tree height (H) and diameter at breast height (D), along with samples of stems, branches, and foliage, were collected in each sample plot. After drying in a constant-temperature oven until the dry weight did not change, the moisture content of the stems, branches, foliage were calculated using Formula 1. Allometric equations were used to compute the biomass of each aboveground tree (Table 1). Then, we calculated the water content of the trees using Formula 1 and Formula 2. Finally, the field-measured plot-scale AVWS was calculated.

$$W_v = \frac{FW - DW}{FW} \tag{1}$$

$$AVWS = \frac{AGB}{(1 - W_v)} \times W_v \tag{2}$$

where AGB represents aboveground biomass, W_v represents aboveground vegetation moisture content

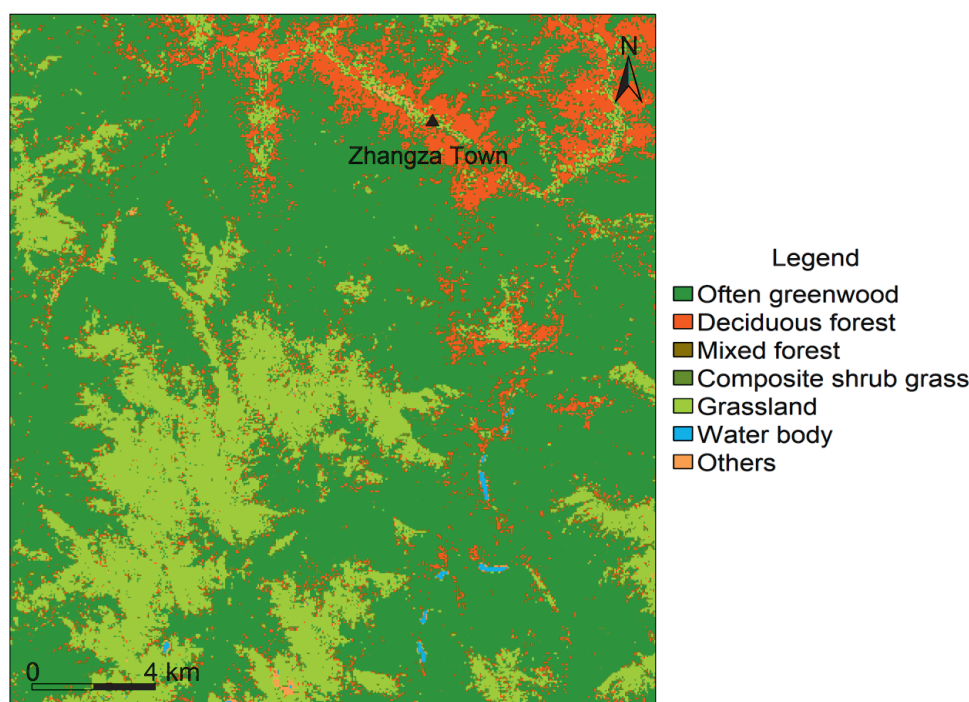


Fig. 2. Surface cover types in the study area.

(percentage form of water content), FW represents fresh weight, and DW represents dry weight. Given parameters D and H, we can use individual allometric equations (Appendix A) to calculate biomass of foliage, stem, and branches that are then used individually and in sum to calculate AVWS.

Considering the forestry and ecology, the field-measured plot-scale AVWS was divided into three parts: the stem, branch, and foliage water contents of the trees. The AVWS of a tree is the sum of AVWS of foliage, branches, and stems. The water content (%) of foliage is calculated using Formula 1, biomass of foliage is calculated using the equations in Appendix A, and AVWS of foliage is calculated using Formula 2. The AVWS calculation of branches and stems is the same as that of foliage. The AVWS of each tree in the sample plot is calculated. Finally, the AVWS of the sample plot is retrieved using remote sensing technology.

Satellite Data Collection and Pre-Processing

S1 and S2 data (Table 1) were downloaded from the official website of the European Space Agency (ESA) Copernicus Open Access Hub. The acquired S1 C-band (5.405 GHz) images were Level-1 Single Look Complex (SLC) products, and collected in the Interferometric Wide (IW) Swath mode. This type of data has VH and VV polarization, and each polarization has three images [24]. The acquired S2 data (Level 1C) carries the optical instrument payload and samples 13 spectral bands: four bands at 10-m, six bands at 20-m, and three bands at 60-m spatial resolution; its spectrum range includes visible light, near infrared, and short-wave infrared. S2 data processing at level 1C includes radiometric and geometric corrections including ortho-rectification and spatial registration on a global reference system with sub-pixel accuracy [25].

The 6.0 version of software SNAP was used to pre-process S1 and S2 data. The S1 preprocessing steps included: (1) calibration; (2) multilooking, (3) speckle reduction, (4) terrain correction. SAR image radiometric calibration corrects the SAR image pixel value to represent the radar backscatter of the reflector, and corrects the incidence angle effect and change of the replica pulse power [26]. In this process, the pixel radiation of the SAR image is calibrated as σ^0 (dB) [27]. Images processed by multilook processing have good interpretability. The Refined Lee Filter and Frost Filter were used to reduce the speckle effect. Finally, SAR images were re-projected to map

projection using the Range-Doppler terrain correction [28] and resampled to 10-m pixel size. The S2 Level-2A image is an orthoimage Bottom-Of-Atmosphere (BOA) corrected reflectance product; S2 Level-1C products should be converted to S2 Level-2A products using the SEN2COR atmospheric correction processor [25]. All pre-processed sentinel images were projected into a common map projection (i.e., UTM 48 WGS84) and resampled to 10-m pixel size.

Modelling the Relationship between Field Water Content and Satellite Data

Sentinel imagery data were divided into three predictor groups: (a) SIG, S1 VH, VV and VH/VV backscattering coefficients; (b) S2G, a total of 10 predictors. There are five vegetation indices (Table 3) and five biophysical indices. The five biophysical indices are: S2-derived vegetation cover biophysical measures (i.e., Leaf Area Index [LAI], Fraction of Absorbed Photosynthetically Active Radiation [FAPAR], fraction of vegetation cover [FCOVER], Chlorophyll content in the leaf [Cab], and canopy water content [CW]), and S2-derived vegetation indices (Table 2), most of which were related to VWC; and (c) For S1G, all predictors in SIG and S2G were used.

In order to establish the best linear model (LM), following the Akaike Information Criterion (AIC) criterion, stepwise regression was carried out using a function step to eliminate collinear variables [26].

The random Forest package in R language was used to establish the optimal Random Forest (RF) regression model. The RF analysis method was used to select the characteristic variables. The optimal number of predictors at the lowest mean square error (MSE) was obtained by Random Forest Cross-Validation, and the IncNodePurity index was used to sort the predictors. Random forests have many decision trees, so by comprehensively analyzing the important information of variables in each decision tree, the final ranking results of importance were obtained. The Random Forest Cross-Validation function and IncNodePurity index were used to determine the optimal predictors for the three modelling groups.

We used 10-fold cross-validation to evaluate the effectiveness of regression models, then relative root mean square error (rRMSE) [34] and 10-fold cross-validation determination coefficients (R^2) between the observed data and the predicted data were calculated to evaluate the performance of the model [35].

Table 1. List of Sentinel imagery.

Mission	Orbit direction	Data name
S1	Ascending	S1A_IW_SLC_1SDV_20180825T110101_20180825T110128_023402_028BE6_7359
S1	Ascending	S1A_IW_SLC_1SDV_20180825T110126_20180825T110153_023402_028BE6_F2E6
S2		S2A_MSIL1C_20180823T034531_N0206_R104_T48SUB_20180823T073131

Table 2. Spectral indices for predicting vegetation water content.

Spectral index	Formula	Source
NDWI (858,1640)	$(NIR - SWIR1)/(NIR + SWIR1)$	[29]
NDII (858,2130)	$(NIR - SWIR2)/(NIR + SWIR2)$	[30]
EVI	$2.5*(R_{nir} - R_{red})/(R_{nir} + 6R_{red} - 7.5R_{blue} + 1)$	[31]
SR	R_{1600}/R_{820}	[32]
NDVI	$(R_{nir} - R_{red})/(R_{nir} + R_{red})$	[33]

$$RMSE = \sqrt{\frac{1}{n} \sum_{i=1}^n (m_i - p_i)^2} \tag{3}$$

$$rRMSE = \frac{RMSE}{\bar{m}} \tag{4}$$

$$R^2 = 1 - \frac{\sum_{i=1}^n (m_i - p_i)^2}{\sum_{i=1}^n (m_i - \bar{m})^2} \tag{5}$$

Where, m_i represents the measured value, p_i represents the predicted value of the model, and \bar{m} represents the average value of the measured value.

Results and Discussion

Measured Aboveground Vegetation Water Storage

The field-measured AVWS ranged between 0.41 and 424.75 (mean = 166.86 t ha⁻¹; standard deviation = 107.18 t ha⁻¹). Considering the different vegetation types, the AVWS of often greenwood was generally higher, followed by that corresponding to mixed forest, deciduous forest, composite shrub grass, and grassland (Fig. 3). Mean water content of the stems was the highest, followed by that of the branches and foliage (Table 3).

This study produced a more accurate inversion of AVWS, which is conducive to more accurate assessment of water resource reserves and regulation mechanisms of vegetation. The hydrological functioning of vegetation [36] makes it closely related to hydrological processes [37]; therefore, the study of AVWS is very helpful for exploring the hydrological function of vegetation.

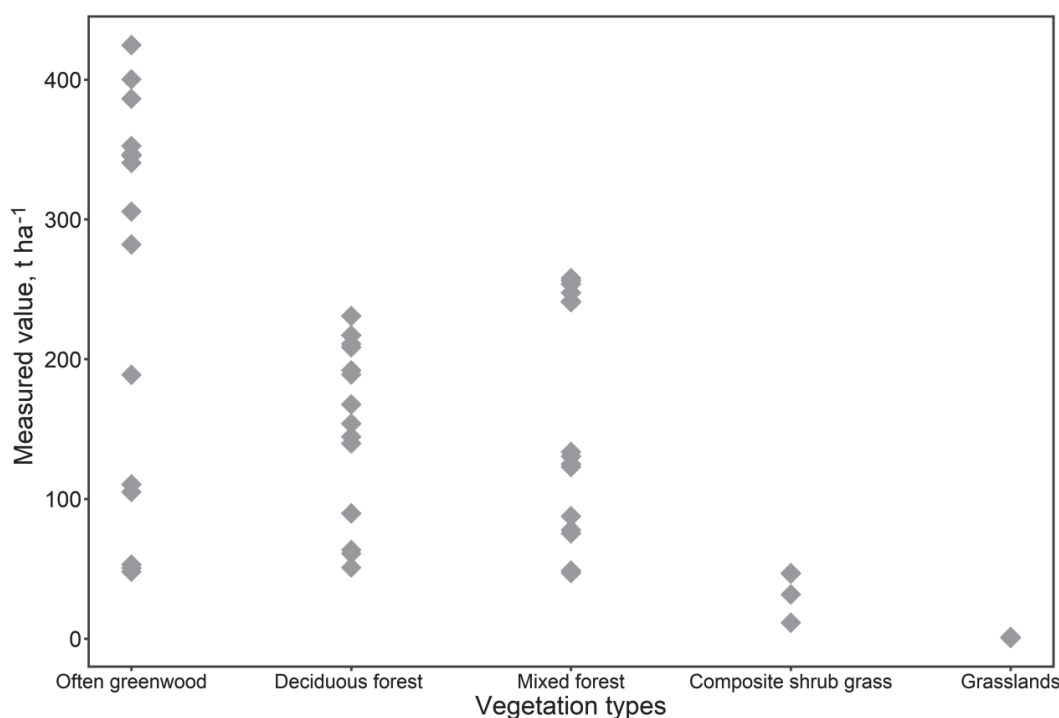


Fig. 3. AVWS of different vegetation types.

Table 3. Mean water content of foliage, branches, and stems by forest type.

Vegetation types	Water content of foliage (t ha ⁻¹)	Water content of branches (t ha ⁻¹)	Water content of stems (t ha ⁻¹)	Average AVWS (t ha ⁻¹)
Evergreen forest	42.6	89.32	117.39	249.31
Deciduous forest	24.53	46.06	80.78	151.37
Mixed forest	32.14	44.7	79.56	156.4
Composite shrub grassland	/	/	/	34.14
Grassland	/	/	/	0.48

However, the water content of plant roots and soil in the root zone were not calculated; this will be the focus of future study.

Linear Regression

An optimal linear prediction model for the three modeling groups, as established (Formula 6-8) based on S2G, was slightly better than those based on S1G; however, the results obtained by combining S1G and S2G were the best (Table 4).

$$AVWS(S1G) = 486.837 + 2.65 \times VH - 54.656 \times VH/VV \quad (6)$$

$$AVWS(S2G) = -80.846 - 106.533 \times NDWI - 6.054 \times FCOVER + 7864.051 \times CW \quad (7)$$

$$AVWS(S12G) = -60.131 - 88.293 \times NDVI - 0.266 \times VH - 208.795 \times NDWI - 2.22 \times FCOVER + 7696.89 \times CW \quad (8)$$

It was also found that most of the optimum variables in S1G were associated with VH polarization. For the cross-polarized VH, the total backscatter contained abundant vegetation scattering information [38] as VH polarization is sensitive to vegetation volume and vegetation density [39]. In the future, we will attempt to use VH polarized SAR data. It can also be seen that among the three linear models, the predictor in S12G is the best because predictors extracted from S1 and S2 images to compensate for radiation and reflection information and improve the accuracy of the AVWS.

Random Forest Regression

The RF prediction model established by the S12G predictors (Fig. 4) had the best variable number determined by MSE. Fig. 5 shows the best variable

determined by IncNodePurity. The final S12G model prediction factors in descending order of importance were NDWI, the FCOVER, VH, NDII, and NDVI. These optimal S12G predictors were then used for further analysis. When the mtry of the S12G model was 7, the accuracy of the S12G model was the highest. Fig. 6 shows a scatter plot between the measured and estimated AVWS, for which the S12G model ($R^2 = 0.72$, rRMSE = 11.94%) is better than that of S1G and S2G (Table 5). Based on the results of the paired t-test ($p > 0.05$), there was no significant difference between the measured and estimated AVWS.

A large number of predictors in four groups were derived from S1 and S2 imagery. When these predictors were used in the LMs and RF regression models to predict water content, two methods were used to select suitable variables. Based on MSE values, suitable predictors can be effectively selected to establish the RF prediction model for predicting water content. If we do not select the appropriate numbers of variables, it becomes difficult to compute when a large number of predictors are used as images, especially when a non-linear model is used to build a prediction map of the target area. We used MSE to select a suitable number of characteristic variables for the RF model to predict water content. In the future, these characteristic variables could also be used to construct other non-linear models.

The advantage of RF modelling is that it can identify non-linear relationships without any explanation of the relationship between input variables and response variables [16]. The R^2 of the RF prediction models of S1 and S2 data were higher than those of the linear models. One of the reasons is the uniform random distribution of the samples in the study area. The AVWS predicted by the RF model did not show too much or too little fitting; therefore, RF modelling is most suitable for AVWS mapping in the study area.

Water Content Predictive Mapping

We found that the RF regression models were superior to the LMs; therefore, RF regression models based on S2G and S12G were selected for mapping AVWS in the study area (Fig. 7).

Table 4. Evaluation of linear models (LMs) for four groups.

Modelling group	R^2	rRMSE (%)
S1G	0.19	23.62
S2G	0.42	19.17
S12G	0.58	15.1

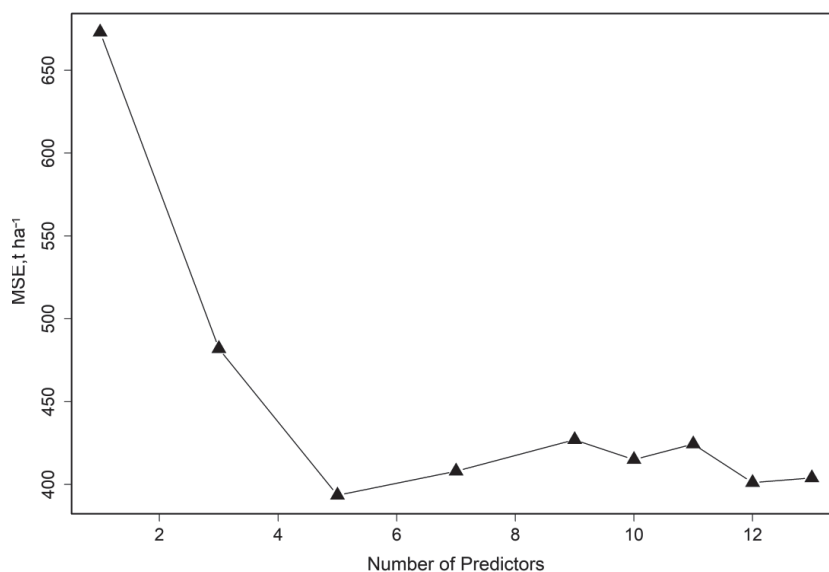


Fig. 4. Best variables number determined by mean square error (MSE).

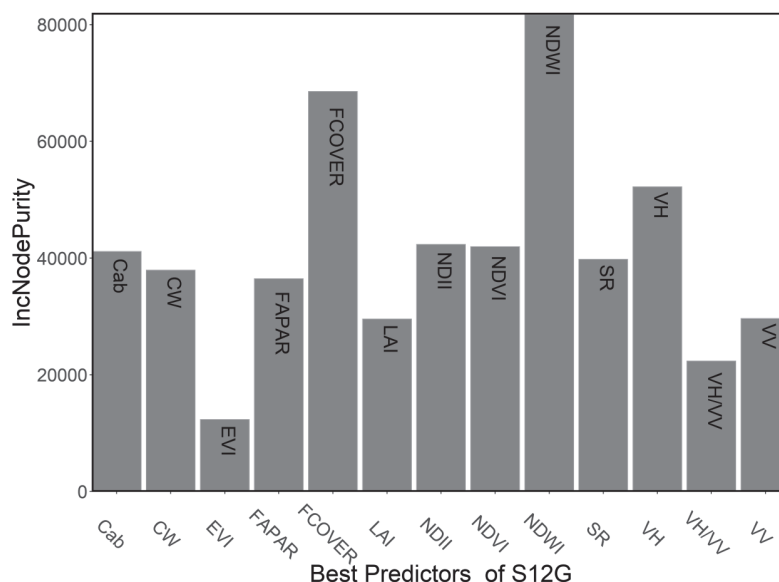


Fig. 5. Best variables of S12G.

From the retrieved AVWS, it was observed that the AVWS of forest land was higher than that of grassland. The major reason for this is that the biomass and water storage volume of the forest canopy were greater than those of grassland. Although the AVWS of forest land

was high, it did not show that the water conservation capacity of forest land was higher than that of grassland, because the water conservation capacity of vegetation included the water volume of the root soil layer, which was not calculated. The water volume of the vegetation root soil layer should be studied in the future.

Table 5. Predictors and evaluation of Random Forest (RF) regression models for four groups.

Modelling group	R ²	rRMSE (%)
S1G	0.34	20.89
S2G	0.67	13.78
S12G	0.72	11.94

It can also be concluded that the forest AVWS retrieved using the spectral group (S2G) predictors was greater than that retrieved using the S1G predictor. The forest AVWS retrieved using the spectral group (S2G) predictor was evenly distributed, representing a rough AVWS, whereas the forest AVWS retrieved by S12G was unevenly distributed, which was comprehensive and close to the actual AVWS. This was because microwaves exhibited certain penetration levels to the

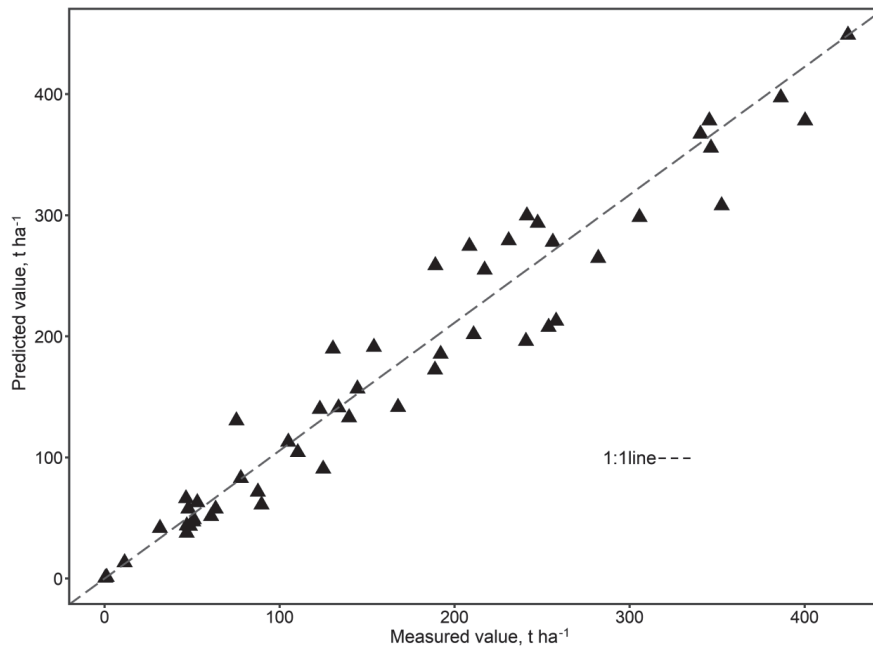


Fig. 6. Scatter plot between the measured and estimated aboveground vegetation water content (AVWS, t ha⁻¹) from Random Forest (RF) regression models based on S12G with a 1:1 line added.

forest canopy and better retrieved the water content of branches and stems under the forest canopy. When the forest canopy is dense, optical remote sensing primarily obtains the surface spectral information of the forest canopy; however, the internal information of the canopy is not effectively obtained, resulting in the AVWS retrieved by S2G failing to completely represent the water content of branches, stems, and some foliage under the canopy. Briefly, optical remote sensing uses the surface spectral information of the canopy to retrieve AVWS, and there is a large difference in the water content of the stems and branches of different

trees. Using only the spectral information of the canopy surface layer led to a small difference in AVWS of different trees, forming a rough and uniform AVWS.

Although the S1 microwave had a certain level of penetration into the forest canopy and grass and effectively obtained the water content of some branches and stems of trees, S1 could not obtain the spectral information of plants. Owing to the existence of shadow and lay-over phenomena in satellite imaging, when an observed object exists in the shadow area of the image in one direction, it may be normal and uncovered in another direction. The results show that our proposed

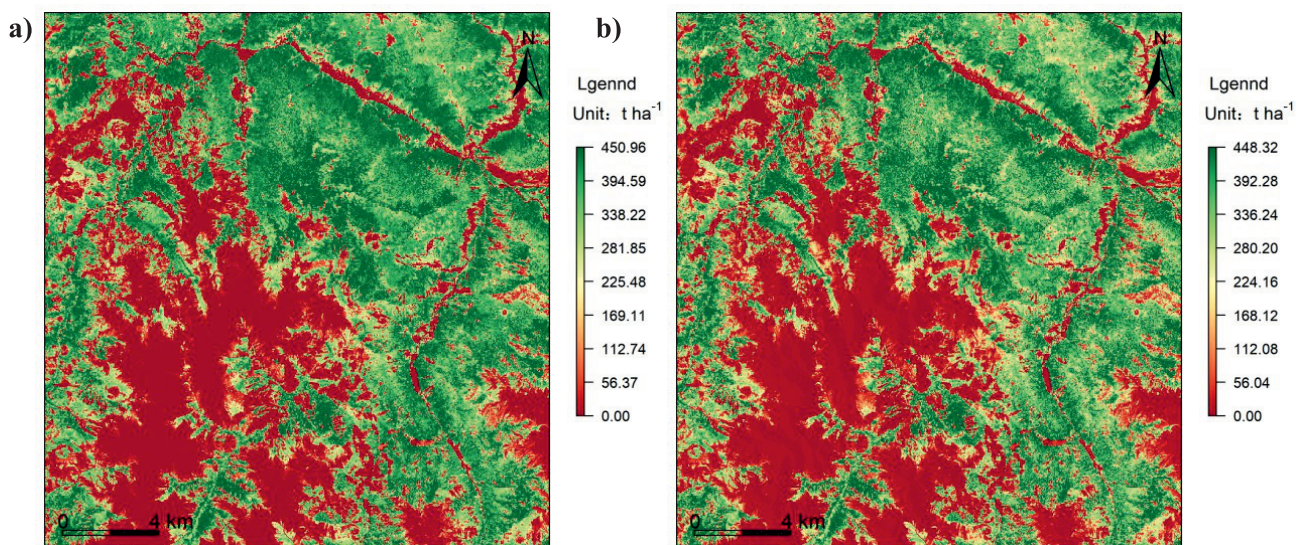


Fig. 7. Predicted maps of aboveground vegetation water content (AVWS; t ha⁻¹) in the study area derived from a) S2G, b) S12G.

method of calculating AVWS improves the accuracy of quantitative inversion; however, S1 and S2 data need to be combined. The AVWS retrieved by S12G can better reflect the water content of some aboveground trees and grass, because the prediction factors of the S12G group consider not only the spectral information of the plant surface layer, but also the three-dimensional spatial structure information of plants (e.g., inside the forest canopy). Therefore, the combination of S1 and S2 data is conducive to the acquisition of effective radiation and reflection information for observation targets.

Conclusions

This work used S1 and S2 imagery to estimate and map the AVWS of Jiuzhaigou Nature Reserve.

Field-measured plot-scale AVWS was calculated, then predictors extracted from S1 and S2 imagery were divided into three modelling groups. A RF regression model based on S12G and S2G were selected for mapping AVWS in the study area. We found that S1 VH polarization is significantly correlated with vegetation water content. Our approach provides a good reference when using S1 and S2 data for inversion of targets. In this study, the LMs and RF regression models established by S12G were better than those established by S1G and S2G. In future remote sensing inversion of vegetation water content, we can apply optical and microwave remote sensing technology to fully retrieve the real water content in vegetation.

Appendix

Appendix A. Allometric equations for calculating the aboveground biomass (AGB) of each tree.

Tree Species	Equations*	R ²	Source
Cypress	$W_s = 0.0754 (D^2H)^{0.7934}$	0.89	[40]
	$W_b = 0.035 (D^2H)^{0.7119}$	0.91	
	$W_f = 0.0685 (D^2H)^{0.6583}$	0.92	
Pinus tabuliformis	$\ln (W_s) = -1.6458 + 0.7626 \ln (D^2H)$	0.87	[41]
	$\ln (W_b) = -4.6813 + 0.8824 \ln (D^2H)$	0.55	
	$\ln (W_f) = -4.4325 + 0.7166 \ln (D^2H)$	0.53	
Abies	$W_s = 0.0139 (D^2H)^{1.0075}$	0.99	[42]
	$W_b = 0.0014 (D^2H)^{1.0503}$	0.91	
	$W_f = 0.0003 (D^2H)^{1.2032}$	0.93	
Picea purpurea	$W_s = 3.166 (D^2H)^{0.4537}$	0.88	[43]
	$W_b = 12.4382 (D^2H)^{0.1928}$	0.91	
	$W_f = 2.9259 (D^2H)^{0.3129}$	0.91	
Pinus densata	$\ln (W_s) = -4.1313 + 2.8571 \ln (D^2H)$	0.84	[44]
	$\ln (W_b) = -4.5868 + 2.4942 \ln (D^2H)$	0.61	
	$\ln (W_f) = -2.5997 + 1.6194 \ln (D^2H)$	0.54	
Betula platyphylla	$W_s = 0.0347 (D^2H)^{0.8714}$	0.86	[42]
	$W_b = 0.0061 (D^2H)^{0.9925}$	0.86	
	$W_f = 0.0189 (D^2H)^{0.6693}$	0.83	
Quercus liaotungensis	$\ln (W_s) = 0.85136 \ln (D^2H) - 3.00984$	0.96	[45]
	$\ln (W_b) = 3.09503 \ln (D^2H) - 5.31497$	0.81	
	$\ln (W_f) = 2.17397 \ln (D^2H) - 1.93175$	0.81	
A very small number of broadleaf trees	$W_s = 5.8252 (D^2H)^{0.0097}$	0.99	[42]
	$W_b = 3.508 (D^2H)^{0.0051}$	0.98	
	$W_f = 0.7563 (D^2H)^{0.0004}$	0.93	

* W_s , W_b , and W_f represent the biomasses of stem, branch and foliage, respectively.

Acknowledgments

This study was supported by the National Natural Science Foundation of China (“Remote Sensing Dynamic Monitoring Method of Vegetation Water content and Water Stress in West Sichuan Plateau”; grant number 41671432) and Key Scientific Research Project Plan of Henan higher Education institutions (“Study on the Coupling Relationship between Economy and Ecological Environment in the Complex Geographical Environment of the Yellow River Basin Based on Remote Sensing Technology”; grant number 23B420002) and Open Foundation of the Research Center for Human Geography of Tibetan Plateau and Its Eastern Slope (“Study on the Coupling Relationship between Economy and Ecological Environment in the Complex Geographical Environment of the Eastern Slope of the Tibetan Plateau Based on Remote Sensing Technology”; grant number RWDL2022-YB002). We thank the anonymous reviewers and editors for their valuable comments and helpful suggestions. We would like to thank Editage (www.editage.cn) for English language editing.

Conflict of Interest

The authors declare no conflict of interest.

References

- NEINAVAZ E., SCHLERF M., DARVISHZADEH R., GERHARDS M., SKIDMORE A.K. Thermal infrared remote sensing of vegetation: Current status and perspectives, *International Journal of Applied Earth Observation and Geoinformation*. **102**, 102415, **2021**.
- DAMM A., COGLIATI S., COLOMBO R., FRITSCHE L., GENANGELI A., GENESIO L., HANUS J., PERESSOTTI A., RADEMSKE P., RASCHER U., SCHUETTEMAYER D., SIEGMANN B., STURM J., MIGLIETTA F. Response times of remote sensing measured sun-induced chlorophyll fluorescence, surface temperature and vegetation indices to evolving soil water limitation in a crop canopy, *Remote Sensing of Environment*. **273**, 112957, **2022**.
- SHAN N., ZHANG Y., CHEN J.M., JU W., MIGLIAVACCA M., PEÑUELAS J., YANG X., ZHANG Z., NELSON J. A., GOULAS Y. A model for estimating transpiration from remotely sensed solar-induced chlorophyll fluorescence, *Remote Sensing of Environment*. **252**, 112134, **2021**.
- CHENG H., WANG J., DU Y., ZHAI T., FANG Y., LI Z. Exploring the potential of canopy reflectance spectra for estimating organic carbon content of aboveground vegetation in coastal wetlands, *International Journal of Remote Sensing*. **42** (10), 3850, **2021**.
- LEI J., YANG W., LI H., WU M., SHE J., ZHOU X., HUANG B., ZHANG Y., LIU L., LUO X. Leaf equivalent water thickness assessment by means of spectral analysis and a new vegetation index, *Journal of Applied Remote Sensing*. **13** (3), 1, **2019**.
- OVEISGHARAN S., HADDAD Z., TURK J., RODRIGUEZ E., LI L. Soil Moisture and Vegetation Water Content Retrieval Using QuikSCAT Data, *Remote Sensing*. **10** (4), 15, **2018**.
- ZHANG Y., SHAO Z. Assessing of Urban Vegetation Biomass in Combination with LiDAR and High-resolution Remote Sensing Images, *International Journal of Remote Sensing*. **42** (3), 964, **2021**.
- JIAO W., WANG L., MCCABE M.F. Multi-sensor remote sensing for drought characterization: current status, opportunities and a roadmap for the future, *Remote Sensing of Environment*. **256**, 112313, **2021**.
- ESPINOZA C.Z., KHOT L. R., SANKARAN S., JACOBY P.W. High Resolution Multispectral and Thermal Remote Sensing-Based Water Stress Assessment in Subsurface Irrigated Grapevines, *Remote Sensing*. **9** (9), **2017**.
- SANDEEP P., REDDY G.O., JEGANKUMAR R., KUMAR K.A.J.E.I. Monitoring of agricultural drought in semi-arid ecosystem of Peninsular India through indices derived from time-series CHIRPS and MODIS datasets, *Ecological Indicators*. **121**, 107033, **2021**.
- ZHENG X., DING Y., ZHAO X., BAI Y., LI X., ZHAO K., JIANG T. Uncertainty evaluation at three spatial scales for the NDVI-based VWC estimation method used in the SMAP algorithm, *Remote Sensing Letters*. **10** (6), 563, **2019**.
- CHRISTOPH S., THOMAS J., MARTIN B., CHRISTIAN T., MARIE P., JEAN-PIERRE W., MARIA P., DARA E. Analysis of the Radar Vegetation Index and Potential Improvements, *Remote Sensing*. **10** (11), 1776, **2018**.
- BERGER K., RIVERA CAICEDO J. P., MARTINO L., WOCHER M., HANK T., VERRELST J. A Survey of Active Learning for Quantifying Vegetation Traits from Terrestrial Earth Observation Data, *Remote Sensing*. **13** (2), 287, **2021**.
- PAN H., CHEN Z., REN J., LI H., WU S. Modeling Winter Wheat Leaf Area Index and Canopy Water Content With Three Different Approaches Using Sentinel-2 Multispectral Instrument Data, *Ieee Journal of Selected Topics in Applied Earth Observations and Remote Sensing*. **12** (2), 482, **2019**.
- WOCHER M., BERGER K., DANNER M., MAUSER W., HANK T. Physically-Based Retrieval of Canopy Equivalent Water Thickness Using Hyperspectral Data, *Remote Sensing*. **10** (12), **2018**.
- MARIETTE V., WOLFGANG W., BERNHARD B.-M., ISABELLA P., IRENE T., CHRISTOPH R., PETER S. Sensitivity of Sentinel-1 Backscatter to Vegetation Dynamics: An Austrian Case Study, *Remote Sensing*. **10** (9), 1396, **2018**.
- TASSI A., VIZZARI M. Object-Oriented LULC Classification in Google Earth Engine Combining SNIC, GLCM, and Machine Learning Algorithms, *Remote Sensing*. **12** (22), 3776, **2020**.
- PULVIRENTI L., SQUICCIARINO G., CENCI L., BONI G., PIERDICCA N., CHINI M., VERSACE C., CAMPANELLA P. A surface soil moisture mapping service at national (Italian) scale based on Sentinel-1 data, *Environmental Modelling & Software*. **102**, 13, **2018**.
- DE ZAN F., GOMBA G. Vegetation and soil moisture inversion from SAR closure phases: First experiments and results, *Remote Sensing of Environment*. **217**, 562, **2018**.
- BOUSBIH S., ZRIBI M., LILI-CHABAANE Z., BAGHDADI N., EL HAJJ M., GAO Q., MOUGENOT B. Potential of Sentinel-1 Radar Data for the Assessment

- of Soil and Cereal Cover Parameters, Sensors (Basel, Switzerland). **17** (11), **2017**.
21. HUANG S., TANG L., HUPY J. P., WANG Y., SHAO G. A commentary review on the use of normalized difference vegetation index (NDVI) in the era of popular remote sensing, Journal of Forestry Research. **32** (1), 1, **2021**.
 22. SANTORO M., CARTUS O. Research Pathways of Forest Above-Ground Biomass Estimation Based on SAR Backscatter and Interferometric SAR Observations, Remote Sensing. **10** (4), **2018**.
 23. ZHANG X., LIU L., CHEN X., XIE S., GAO Y. Fine Land-Cover Mapping in China Using Landsat Datacube and an Operational SPECLib-Based Approach, Remote Sensing. **11**, 1056, **2019**.
 24. MA C., JOHANSEN K., MCCABE M.F. Monitoring Irrigation Events and Crop Dynamics Using Sentinel-1 and Sentinel-2 Time Series, Remote Sensing. **14** (5), 1205, **2022**.
 25. SENTINEL-2_TEAM., Sentinel-2 User Handbook, European Space Agency. **2015**.
 26. CASTILLO J.A.A., APAN A.A., MARASENI T.N., SALMO S.G. Estimation and mapping of above-ground biomass of mangrove forests and their replacement land uses in the Philippines using Sentinel imagery, Isprs Journal of Photogrammetry and Remote Sensing. **134**, 70, **2017**.
 27. SANTOS-FERREIRA A.M., DA SILVA J.C.B., MAGALHAES J.M., SAR Mode Altimetry Observations of Internal Solitary Waves in the Tropical Ocean Part 1: Case Studies, Remote Sensing. **10** (4), 644, **2018**.
 28. VECI L. Sentinel-1 Toolbox: SAR Basics Tutorial, ARRAY Systems Computing, Inc and European Space Agency. **2015**.
 29. DONOVAN S.D., MACLEAN D.A., ZHANG Y., LAVIGNE M.B., KERSHAW J.A. Evaluating annual spruce budworm defoliation using change detection of vegetation indices calculated from satellite hyperspectral imagery, Remote Sensing of Environment. **253**, 112204, **2021**.
 30. LIU F., LIU H., XU C., ZHU X., HE W., QI Y. Remotely sensed birch forest resilience against climate change in the northern China forest-steppe ecotone, Ecological Indicators. **125**, 107526, **2021**.
 31. HUETE A., DIDAN K., MIURA T., RODRIGUEZ E.P., GAO X., FERREIRA L.G. Overview of the radiometric and biophysical performance of the MODIS vegetation indices, Remote Sensing of Environment. **83** (1-2), 195, **2002**.
 32. CECCATO P., FLASSE S., TARANTOLA S., JACQUEMOUD S., GRÉGOIRE J.-M. Detecting vegetation leaf water content using reflectance in the optical domain, Remote Sensing of Environment. **77** (1), 22, **2001**.
 33. TUCKER C.J. Red and photographic infrared linear combinations for monitoring vegetation, Remote Sensing of Environment. **8** (2), 127, **1979**.
 34. LEI J., YANG W., YANG X. Soil Moisture in a Vegetation-Covered Area Using the Improved Water Cloud Model Based on Remote Sensing, Journal of the Indian Society of Remote Sensing. **50** (1), 1, **2022**.
 35. HALME E., PELLIKKA P., MOTTUS M. Utility of hyperspectral compared to multispectral remote sensing data in estimating forest biomass and structure variables in Finnish boreal forest, International Journal of Applied Earth Observation and Geoinformation. **83**, **2019**.
 36. DRASTIG K., SUÁREZ QUIÑONES T., ZARE M., DAMMER K.-H., PROCHNOW A. Rainfall interception by winter rapeseed in Brandenburg (Germany) under various nitrogen fertilization treatments, Agricultural and Forest Meteorology. **268**, 308, **2019**.
 37. WANG H., TETZLAFF D., BUTTLE J., CAREY S.K., LAUDON H., MCNAMARA J.P., SPENCE C., SOULSBY C. Climate-phenology-hydrology interactions in northern high latitudes: Assessing the value of remote sensing data in catchment ecohydrological studies, Science of The Total Environment. **656**, 19, **2019**.
 38. BAO Y.S., LIN L.B., WU S.Y., DENG K.A.K., PETROPOULOS G.P. Surface soil moisture retrievals over partially vegetated areas from the synergy of Sentinel-1 and Landsat 8 data using a modified water-cloud model, International Journal of Applied Earth Observation and Geoinformation. **72**, 76, **2018**.
 39. GAO Q., ZRIBI M., ESCORIHUELA M.J., BAGHDADI N. Synergetic Use of Sentinel-1 and Sentinel-2 Data for Soil Moisture Mapping at 100 m Resolution, Sensors. **17** (9), **2017**.
 40. SHI P., ZHONG Z., LI X. A Study on the Biomass of Alder and Cypress Artificial Mixed forest in Sichuan, Acta Phytoecologica Sinica. **20** (6), 524, **1996**.
 41. MA Q. A Study on the Biomass of Chinese Pine Forests, Journal of Beijing Forestry University. (4), 1, **1989**.
 42. LUO T., SHI P., JI LUO, OU Y. Distribution Patterns of Aboveground Biomass in Tibetan Alpine Vegetation Transects, Acta Phytoecologica Sinica. **26** (6), 668, **2002**.
 43. JIANG H. A study on the biomass and production of picea purpurea frost communities, Acta Phytoecologica Sinica. **10** (2), 146, **1986**.
 44. WANG Y., MA Q., HOU G., BAN Z., CHEN Y., Dynamics of Biomass and Productivity in the Natural Restoration Progress of the Pinus densata Burned Areas in Western Sichuan Province., Forestry Science & Technology. **32** (1), 37, **2007**.
 45. ZHANG B., Study on Biomass and Productivity of Quercus lidotungensis Stands in Ziwuling Forest Region of Shaanxi Province, Journal of Northwest Forestry University. (1), 1, **1990**.